IEEE Transactions on Quantum Engineering

Received 22 February 2025; revised 9 July 2025; accepted 26 July 2025; date of publication 4 August 2025; date of current version 4 September 2025.

Digital Object Identifier 10.1109/TQE.2025.3595706

TCEP-Based Synchronization for Practical Communication Network

SWARAJ SHEKHAR NANDE[1] (Member, IEEE), SHUBH AGARWAL[2], STEFAN KRAUSE[3], RICCARDO BASSOLI[1] (Senior Member, IEEE), KAY-UWE GIERING[3,4], KOTESWARARAO KONDEPU[2] (Senior Member, IEEE), AND FRANK H.P. FITZEK[1] (Fellow, IEEE)

[1]Deutsche Telekom Chair of Communication Networks, TU Dresden, 01069 Dresden, Germany
[2]Department of Computer Science and Engineering, IIT Dharwad, Dharwad, Karnataka 580011, India
[3]Fraunhofer Institute for Integrated Circuits (IIS), Division EAS, 01187 Dresden, Germany
[4]Electrical Engineering Department, HTW Dresden, 01069 Dresden, Germany

Corresponding author: Swaraj Shekhar Nande (e-mail: swaraj_shekhar.nande@tu-dresden.de).

This work was supported in part by the Federal Ministry of Education and Research of Germany in the programme of "Souverän. Digital. Vernetzt.". Joint project 6G-life project identification: 16KISK001K, in part by the German Research Foundation (DFG, Deutsche Forschungsgemeinschaft) as part of Germany's Excellence Strategy – EXC2050/1 – Project ID 390696704 – Cluster of Excellence "Centre for Tactile Internet with Human-in-the-Loop" (CeTI) of Technische Universität Dresden, in part by the Federal Ministry of Education and Research of Germany in the project QD-CamNetz project identification: 16KISQ076K, in part by the Federal Office for Information Security of Germany in the project QSyncNextG, project identification: 01MO23031C, and in part by the Federal Ministry of Education and Research of Germany in the project QUARKS project identification 16KIS1998K. The work of Stefan Krause and Kay-Uwe Giering was supported in part by the European Regional Development Fund and in part by the state budget passed by the Saxon state parliament under Grant 100498890, Grant 100498868, and Grant 4-7324/27/3-2022/32856.

ABSTRACT Precise time synchronization is a fundamental challenge in distributed quantum systems, with direct implications for secure communication, quantum sensing, and next-generation quantum network technologies. In this work, we present an field programmable gate arrays (FPGA)-based implementation of a synchronization system using time-correlated entangled photons (TCEP), achieving timing precision below 200 ps across 10- and 20-km deployed fiber links using spectral filtering (SF) and dispersion compensation. The system exploits the intrinsic temporal correlations of entangled photon pairs to estimate synchronization offsets between remote nodes. A modular architecture is developed, featuring optimized OpenCL kernels for real-time correlation, timestamp aggregation, and peak normalization. This enables high-throughput performance with efficient utilization of hardware resources. Experimental validation confirms that the FPGA processes entangled photon timestamps and computes cross-correlation functions significantly faster than conventional CPU-based methods, achieving execution times in the range of a few milliseconds for datasets containing up to 10^5 timestamped events per node. Resource utilization analysis further demonstrates the scalability of the design, with the system operating reliably at a 397.5-MHz clock frequency while maintaining efficient logic, register, and memory usage. Our results illustrate the feasibility of deploying FPGA-based TCEP synchronization in real-world quantum networks, supporting applications in ultra-reliable low-latency communication, distributed quantum computing, and quantum-enhanced localization and sensing. This work bridges foundational quantum photonic principles and hardware-level deployment, laying the groundwork for timing infrastructure in future quantum internet and 6G networks.

INDEX TERMS Distributed computing, network synchronization, optical fiber communication, quantum communication, quantum correlation, quantum-enhanced sensing and navigation, secure communication, time synchronization, ultra-reliable low-latency communication.

I. INTRODUCTION

The rapid advancements in distributed systems, encompassing quantum communication networks, ultra-reliable low-latency communication (URLLC), and autonomous technologies have intensified the demand for clock-synchronization with subnanosecond precision. In addition, applications, such as secure communication, real-time decision-making in autonomous systems, and high-frequency financial transactions rely on precise timing to ensure data integrity, system reliability, and operational security. However, achieving this level of synchronization remains a challenge despite decades of progress.

Classical synchronization methods, including the network time protocol (NTP) and precision time protocol (PTP), have been pivotal in modern networks. PTP (IEEE 1588) achieves nanosecond-level accuracy through hardware timestamping. However, its performance is constrained by network-induced jitter and delay asymmetry, particularly in large-scale or geographically dispersed networks [4]. These limitations have prompted researchers to explore novel synchronization techniques that leverage optical and quantum phenomena.

One of the most notable developments in classical synchronization is the White Rabbit (WR) protocol, which integrates synchronous Ethernet (SyncE) with PTP. Initially developed at CERN for time-critical scientific experiments, WR achieved synchronization precision within tens of picoseconds over Ethernet networks [30]. WR extends IEEE 1588-2008 PTP by incorporating link asymmetry compensation, syntonization via SyncE, and precise phase alignment using dual-mixer time difference modules. These improvements have enabled WR to demonstrate subnanosecond accuracy over fiber links spanning beyond 10 km and in cascaded chains of up to 15–20 nodes [16], [33].

However, the accuracy of WR depends on hardware calibration and controlled environments. Its performance degrades in long daisy-chain topologies due to cumulative jitter and frequency offsets. As more layers and nodes are added, synchronization components, such as phase-locked loops introduce additional jitter, which can impact overall timing precision.

While WR offers scalability in classical networks, its end-to-end delay model introduces synchronization drift, which poses challenges in decentralized and dynamic environments, such as quantum networks. Recent approaches using peer-to-peer transparent clocks and hybrid clock modes have improved WR's stability and scalability, but fundamental architectural constraints remain [16].

Quantum-based synchronization techniques have emerged as promising alternatives, with quantum states offering the potential to surpass classical limits. Entanglement ensures that the states of two particles remain correlated across large distances, thus providing a shared reference for clock synchronization. The authors of the theoretical studies in [14] and [20] demonstrated that entanglement can provide a shared quantum reference frame between remote nodes, leading to enhanced synchronization performance. These studies also motivated protocols that exploit more general quantum correlations, including time-energy entanglement and purely time-correlated photon pairs, which can be realized through spontaneous parametric down conversion (SPDC) [31].

Time-correlated entangled photons (TCEP) generated through SPDC in nonlinear crystals [28] can be instrumental in demonstrating the practical feasibility of quantum synchronization, as it enables the establishment of a shared time reference between remote nodes without the need for a centralized timing source, and is robust against environmental disturbances.

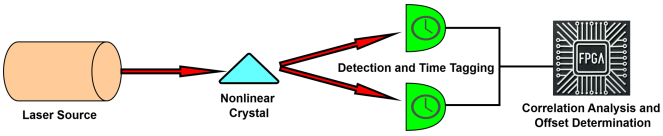

FIGURE 1. Schematic of the TCEP-based synchronization process between Alice and Bob. The temporal correlation of the entangled photon pairs enables precise time synchronization. The offset between Alice and Bob's local clocks is calculated on FPGA.

By exploiting the inherent temporal correlations between entangled photon pairs, Valencia et al. [34] achieved picosecond-level clock synchronization. TCEP-based synchronization offers significant benefits, including better scalability and resistance to environmental disturbances, making it an ideal choice for large-scale quantum network applications [31]. It permits the identification of events that have occurred simultaneously at a shared node and then been propagated toward the two communicating parties, Alice and Bob, thereby correcting for effects, such as clock frequency mismatches, clock offsets, and different optical path lengths, including their temporal fluctuations.

TCEP source-based synchronization inherently supports wavelength-division multiplexing (WDM), enabling quantum timing signals to coexist with other quantum or classical channels within a single optical fiber. As it relies exclusively on entangled photon pairs and does not require strong classical synchronization pulses, it circumvents Raman scattering noise that would otherwise degrade neighboring wavelength channels. This makes TCEP particularly well-suited for integration into multiplexed quantum networks. Furthermore, with sufficiently high entangled photon-pair generation rates and picosecond-resolution detectors, this approach enables high-precision clock synchronization over fiber links exceeding 59 km, as demonstrated in recent experiments [21].

The correlation algorithm used to determine the clock offset from the time-tagging datasets does not require entanglement. However, exploiting the entanglement enables an additional distribution of random numbers in the network [quantum key distribution (QKD)]. In addition, verifying the nonclassical correlations allows for an integrity check of the synchronization events that are actually used. In case of high attenuation, filtering for the expected nonclassical correlations can improve the synchronization accuracy. Furthermore, TCEP-based synchronization in a network, i.e., beyond a two-party link, can be made available, for instance, by providing a source of entangled photons as a shared network service and by appropriately splitting its signal into WDM channels for pairwise parallel synchronization of parties, in analogy to QKD in a network structure [36].

A basic systematic diagram of the TCEP process is shown in Fig. 1. To fully utilize TCEP in distributed quantum networks, it is essential to address scalability and real-time processing. Field programmable gate arrays (FPGAs) serve as an excellent solution to meet these requirements, being well known for their parallel processing capabilities, real-time

reconfigurability, and high-throughput performance. FPGAs can efficiently support the computational requirements of TCEP synchronization protocols [22] by operating at clock frequencies exceeding 350 MHz. Further, FPGAs enable real-time adaptation and modularity, making it ideal for large-scale deployment in quantum networks [12].

Beyond synchronization, the TCEP hardware infrastructure can be extended to enable secure communication protocols, such as QKD, further expanding its utility in quantum networks [29]. This article aims to provide advances in classical and quantum synchronization by demonstrating that TCEP source-based synchronization, integrated with FPGA hardware, offers a scalable and robust solution for achieving subnanosecond-level precision with further scope for enhancement. This approach establishes TCEP as a foundational technology for next-generation quantum communication networks, supporting secure, ultra-reliable, and low-latency operations by addressing the critical challenges of real-time processing and scalability.

II. THEORETICAL BACKGROUND

Traditional time synchronization methods in networked systems, such as the NTP and PTP, rely on exchanging time-stamped packets across the network and adjusting for measured delays. While widely used, these methods have several limitations, particularly due to network-induced delays and security vulnerabilities. As fields like quantum communications and high-frequency trading demand higher precision and security, more advanced synchronization techniques have become paramount [10], [25].

A. LIMITATIONS OF CLASSICAL SYNCHRONIZATION TECHNIQUES

Classical time synchronization methods, including the NTP, PTP, and WR, have been foundational to distributed systems. While effective in their respective domains, these methods face significant challenges in addressing the demands of modern applications requiring ultra-precise, scalable, and robust synchronization.

1) *Accuracy Limitations:* NTP, widely used over the public Internet, achieves accuracies of 1–10 ms under typical conditions [9]. While suitable for general-purpose applications, it is insufficient for time-sensitive systems requiring submicrosecond or nanosecond-level precision, such as high-frequency trading or quantum networks. PTP achieves submicrosecond accuracy through hardware timestamping, yet its performance degrades in environments with asymmetric delays and high network variability [6]. The WR protocol, which integrates SyncE with PTP, achieves subnanosecond accuracy; however, its deployment is resource-intensive and relies on specialized infrastructure [26].
2) *Dependency on External Conditions:* Many classical methods rely on external sources, such as GPS, for time references. GPS provides accuracies within ± 10 ns under ideal conditions but is vulnerable to signal obstructions, jamming, and spoofing, particularly in urban or indoor environments [1], [8]. In addition, variable network latencies, ranging from 1–100 ms, introduce significant inconsistencies in synchronization, particularly in large-scale or congested networks [28], [38].
3) *Environmental Sensitivity and Drift:* Timekeeping in classical systems relies heavily on crystal oscillators, which are sensitive to temperature variations. A drift of 0.5 ppm per degree Celsius translates to errors of up to 43 ms per day for each degree of fluctuation, necessitating frequent updates or higher grade oscillators that increase cost and complexity [35].
4) *Scalability Constraints:* In large-scale networks with thousands of nodes, synchronization protocols struggle to maintain consistent timing. The propagation of updates can take several seconds, leading to clock drift and reduced reliability. This challenge is exacerbated in dynamic environments, such as data centers or mobile networks, where frequent topology changes demand higher synchronization rates [7].

B. QUANTUM SYNCHRONIZATION WITH TCEP

TCEP offers a promising quantum-based alternative to classical synchronization methods. TCEP synchronization leverages the entangled photon pair sources, enabling precise synchronization over long distances [28]. The entangled photon pairs are generated through SPDC, a process in which a pump photon interacts with a nonlinear crystal, producing two entangled photons, referred to as the signal and idler photons [2], [3], [11]. The following equations govern the conservation of energy and momentum during the SPDC process:

$$\omega_p = \omega_s + \omega_i \tag{1}$$

$$\vec{k}_p = \vec{k}_s + \vec{k}_i \tag{2}$$

where ω_p, ω_s, and ω_i represent the frequencies of the pump, signal, and idler photons, respectively, and $\vec{k}_p$, $\vec{k}_s$, and $\vec{k}_i$ are their corresponding wave vectors [18].

The primary benefit of utilizing entangled photons for synchronization lies in their inherent temporal correlation. When observed at two different locations, typically referred to as Alice and Bob, the exact timing of the photons' arrival can be used to synchronize the clocks at both locations, as illustrated in Fig. 1.

The time difference in the arrival of the entangled photons at Alice and Bob can be expressed as

$$\Delta t = t_A - t_B - \Theta \tag{3}$$

where t_A and t_B represent the arrival times of the photons at Alice and Bob, respectively, and Θ denotes the propagation delay. The precise timing correlations between photon pairs originate from the SPDC process and remain preserved over

long distances, enabling accurate clock synchronization by measuring and correcting the clock offset Δt.

Furthermore, when entangled photon pairs are employed, the synchronization precision can surpass classical limits due to the enhanced phase sensitivity inherent in quantum correlations. Specifically, entangled states allow for the accumulation of phase information at a rate that scales quadratically with the number of resources, leading to a quantum Fisher information $F_Q \propto N^2$ and a corresponding Heisenberg-limited timing uncertainty of $\Delta t_{\mathrm{HL}} = 1/(N\omega)$, where ω is the optical frequency [15], [19]. In contrast, classical synchronization strategies are constrained by the standard quantum limit (SQL), which scales as $\Delta t_{\mathrm{SQL}} \propto 1/\sqrt{N}$. While recent attosecond-resolved Hong–Ou–Mandel interferometry has demonstrated femtosecond-scale delay resolution using broadband sources and local feedback estimation [24], such methods are inherently local and sensitive to optical path instability. In contrast, TCEP-based protocols are designed for long-distance synchronization over optical fibre links, leveraging the stable temporal correlations of SPDC-produced photons. When implemented with real-time FPGA-based correlation and detection, TCEP not only achieves robust and scalable performance but also retains the potential for Heisenberg-limited scaling in distributed clock synchronization [39].

III. MATHEMATICAL FORMULATIONS

A. TIMING JITTER AND PHOTON DETECTION

The accuracy of the TCEP source-based clock synchronization process depends significantly on the timing jitter linked to detecting individual photons. Timing jitter refers to the uncertainty in determining the precise moment when a photon is detected, resulting from the characteristics of single-photon detectors and related electronics, such as time-to-digital converters (TDCs).

As a consequence, Alice and Bob cannot attribute exactly coinciding timestamps to in principal simultaneous events (such as the emission time of two pair photons in the SPDC process). The root-mean-square (RMS) timing jitter is defined as the standard deviation (σ) of an underlying Gaussian distribution function. It is related to the full width at half maximum (FWHM) of the Gaussian distribution by $\mathrm{FWHM} = 2\sqrt{2\ln 2}\cdot\sigma \approx 2.355\cdot\sigma$.

Several contributing factors influence the overall timing jitter in a TCEP setup as follows.

1) *Single-Photon Detector Jitter:* The intrinsic jitter of single-photon detectors, such as single-photon avalanche diodes (SPADs) or superconducting nanowire single-photon detectors (SNSPDs), can range from tens of picoseconds (for SNSPDs) to a few hundred picoseconds (for SPADs).
2) *TDC Resolution and Jitter:* The timing resolution and jitter introduced by the TDCs affect the measured arrival times of photons. High-resolution TDCs with picosecond-level precision are essential to minimize timing errors in the synchronization process.
3) *Optical Path Variations:* Fluctuations in the optical path due to factors like temperature changes or mechanical vibrations can introduce additional timing uncertainties. These variations can be modeled as stochastic noise in the timing measurements.

The collective impact of these factors causes variations in the timing measurements, ultimately restricting the accuracy of the clock synchronization.

B. COHERENCE TIME AND ITS ROLE IN SYNCHRONIZATION

Another critical parameter in the TCEP synchronization method is the coherence time τ_c of the entangled photon pairs, which is inversely related to the linewidth $\Delta\lambda$ of the SPDC process used to generate the photons

$$\tau_c = \lambda^2/(c\Delta\lambda) \tag{4}$$

with λ being the wavelength of the photon and c the speed of light. In the present case, we use coarse wavelength division multiplexers to separate the entangled photons and feeding them into the fibers toward Alice and Bob, respectively. These multiplexers feature a 20-nm transmission window resulting in a coherence time of about 0.4 ps which is far below the detector and time tagger jitter. However, other sources (Sagnac type) or different types of SF [dense WDM (DWDM)] can lead to narrow spectral linewidths. E.g., 100 GHz are a typical spectral window for DWDMs. This would result in a coherence time of about 10 ps. This value is of the same order of magnitude as the device jitter from high performance detectors and time taggers and needs to be taken into account especially since SF is a widely applied method to avoid correlation broadening due to fiber dispersion.

This balance is crucial in optimizing the performance of TCEP synchronization.

C. CROSS-CORRELATION FUNCTION [23]

The cross-correlation function is an essential tool in TCEP-based synchronization for determining the precise time offset between the clocks at Alice and Bob. It measures how well two time series of photon arrival events, t_A and t_B, align when compared with each other.

To mathematically define the cross-correlation function, let t_i represent the arrival time of the ith photon at Alice, and u_j represent the arrival time of the jth photon at Bob. For discrete photon arrival times, the intensity functions $I_A(t)$ and $I_B(t)$ indicate the number of photons detected at time t at Alice and Bob, respectively. These functions can be formally defined as

$$I_A(t) = n\left(\{i \mid t_i = t\}\right)/\Delta t \tag{5}$$

$$I_B(t) = n\left(\{j \mid u_j = t\}\right)/\Delta t \tag{6}$$

where

IEEE Transactions on Quantum Engineering

- 1) $n(\{i \mid t_i = t\})$ counts the number of photons arriving at time $t_i = t$ at Alice;
- 2) $n(\{j \mid u_j = t\})$ counts the number of photons arriving at time $u_j = t$ at Bob;
- 3) Δt is the time resolution of the measurement.

The first-order cross-correlation function $\hat{C}_{AB}(\tau)$ with discrete time lag τ and for a finite experimental time T is calculated as follows:

$$\hat{C}_{AB}(\tau) = \frac{n\left(\{i \mid t_{Ai} = t_{Bj} - \tau\}\right) T/\Delta t}{n\left(\{i \mid t_{Ai} \leq T + \tau\}\right) \cdot n\left(\{j \mid t_{Bj} \geq \tau\}\right) (T/\Delta t)}. \tag{7}$$

In (7):

- 1) $n(\{i \mid t_{Ai} = t_{Bj} - \tau\})$ counts the number of coincident photon detection events within a specified time window;
- 2) the denominator normalizes the result by accounting for the total number of photons detected within the experimental time T.

The amplitude as a function of the lag time tau τ resembles a Gaussian peak. The peak's expectation value corresponds to the propagation delay Θ. The width of the peak is directly correlated to the timing precision of the measurement devices, as well as any dispersive effects in the optical fiber, fluctuations in the propagation medium, and natural broadening due to the SPDC process.

Determining the exact time offset between Alice and Bob relies on calculating $\hat{C}_{AB}(\tau)$. A large amplitude in the cross-correlation function suggests a stronger correlation between the times the photons arrive, indicating more precise synchronization. The behavior of the function at different τ values gives us insights into the timing accuracy and potential error sources, making it an essential part of the TCEP synchronization process.

In practical terms, calculating cross-correlation involves working with large datasets of photon arrival times, which can be computationally intensive, especially at high photon count rates. However, this process is crucial for achieving the high level of precision necessary in quantum time synchronization. The accuracy of the resulting synchronization is usually assessed by examining the width and shape of the cross-correlation peak, with narrower peaks indicating higher precision.

IV. FIELD PROGRAMMABLE GATE ARRAYS (FPGAS)

FPGAs have evolved from simple reconfigurable devices to advanced platforms capable of handling complex real-time processing tasks, making them integral to high-performance communication networks.

A. EVOLUTION OF FPGAS

FPGAs were first introduced by Xilinx in 1985 as a flexible, reconfigurable alternative to application-specific integrated circuits (ASICs) [5]. While ASICs are tailored for specific tasks and cannot be altered after fabrication, FPGAs allow postfabrication reconfiguration, enabling them to support multiple applications without requiring new hardware designs. Initially, FPGAs were limited to simple control tasks. However, advances, such as the introduction of look-up tables (LUTs) and highly configurable interconnects have expanded their capability for handling more complex functions.

The primary architecture of an FPGA consists of configurable logic blocks (CLBs) connected through programmable interconnects. These CLBs can be configured to execute various logic functions, allowing the FPGA to adapt to different tasks dynamically. Over time, additional resources, such as digital signal processing (DSP) blocks, embedded memory, and high-speed I/O interfaces, have been added, enabling FPGAs to perform real-time processing in advanced applications, including high-performance communication networks [22].

B. FPGAS IN MODERN COMMUNICATION NETWORKS

The advent of 5G, quantum networks, and high-bandwidth optical communication systems has increased the demand for devices capable of handling large amounts of data at high speeds. FPGAs have emerged as an essential technology for these applications due to their parallel processing capabilities and low-latency operation. In communication networks, FPGAs are used to implement functions, such as packet processing, error correction, encryption, and synchronization and are actively investigated for real-time-based processing [37]. Their reprogramming ability allows network operators to adapt to new standards and protocols without changing the underlying hardware, which is particularly important in rapidly evolving fields like quantum communication.

C. MATHEMATICAL FRAMEWORK AND SCIENCE BEHIND FPGA OPERATION

At the core of FPGA operation is the concept of reconfigurable logic. Each CLB within an FPGA is based on LUTs, which implement logic functions. Mathematically, an LUT can be represented as a mapping from a set of inputs to a corresponding output, much like a truth table.

Given an n-input LUT, the number of possible input combinations is 2^n, and the LUT stores the corresponding outputs for each combination. Formally, an LUT implements a Boolean function $f : \{0, 1\}^n \to \{0, 1\}$, where each n-bit input corresponds to a precomputed output stored in the LUT

$$f(x_1, x_2, \ldots, x_n) = \mathrm{LUT}(x_1, x_2, \ldots, x_n). \tag{8}$$

In addition to LUTs, FPGAs utilize multiplexers to control signal routing between different CLBs and Logic elements. The interconnection network is programmed by a set of configuration bits that control which paths are active. The flexibility of these interconnections allows FPGAs to be configured for a wide range of applications.

FPGAs also incorporate specialized blocks, such as DSP units, which are optimized for mathematical operations commonly found in communication systems. These blocks often support high-precision fixed-point or floating-point arithmetic, enabling the implementation of algorithms, such as

fast Fourier transforms, finite impulse response filters, and error correction codes. Mathematically, these DSP blocks can be represented by operations, such as

$$y[n] = \sum_{k=0}^{N-1} h[k]x[n-k] \tag{9}$$

where $h[k]$ represents the filter coefficients, and $x[n]$ is the input signal. This convolution operation is a fundamental part of many signal processing algorithms used in communication systems, including those implemented on FPGAs.

D. TCEP SOURCE-BASED SYNCHRONIZATION USING FPGAS

TCEP provides a quantum-based method for achieving high-precision synchronization across distributed systems. In our implementation, photon pairs generated through SPDC are detected at two distant nodes (e.g., Alice and Bob), and the time stamps of these detection events are recorded. The goal of TCEP-based synchronization is to use the temporal correlations between entangled photon pairs to calculate the time offset between the two nodes.

FPGAs play a central role in this process by collecting timestamps and detection events from both nodes and processing them in real-time. To calculate the time offset between the nodes, we implemented the photon correlation algorithm specified [23] on the FPGA. The algorithm calculates the temporal correlation between detection events at both nodes, enabling us to determine the time delay with high precision.

The correlation function has already been shown in (7). The system can compute the correlation function by processing these timestamps in real time on the FPGA and dynamically adjusting Δt to synchronize the respective nodes. The FPGA parallel processing capabilities enable efficient handling of the high volume of photon detection events, ensuring minimal latency in calculating the correlation function.

The complete architectural description of the test bed is shown in Fig. 2.

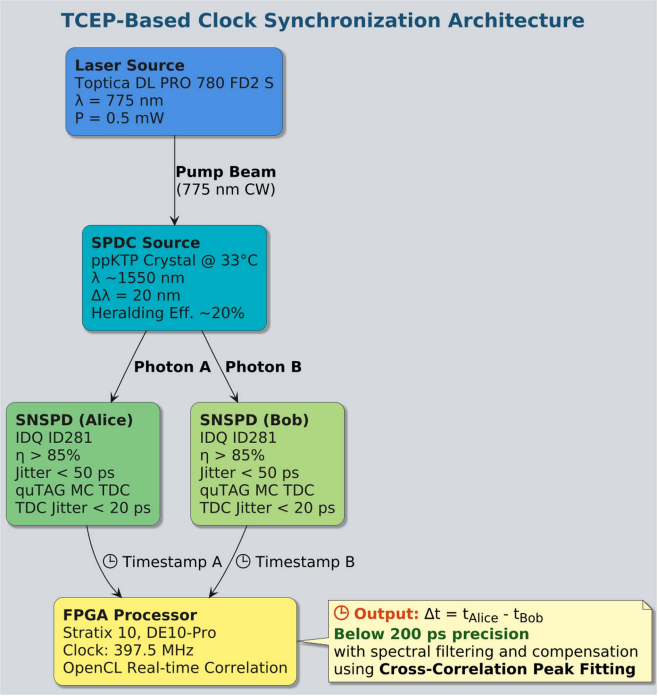

FIGURE 2. TCEP-based clock synchronization complete architecture. A CW laser at 775 nm (Toptica DL PRO 780 FD2 S) with 0.5-mW power pumps a temperature-stabilized periodically poled KTP nonlinear crystal at 33 °C, generating time-correlated entangled photon pairs around 1550 nm with a $\Delta\lambda$ of 20 nm and heralding efficiency of ∼20%. The photon pairs (labeled A and B) are detected by SNSPDs, IDQ ID281 with >85% efficiency and jitter <50 ps. Each detection event is timestamped using a quTAG MC Time-to-Digital Converter with sub-20 ps jitter. These timestamps are processed by a Stratix 10 DE10-Pro FPGA operating at 397.5 MHz and programmed with OpenCL for real-time cross-correlation. By applying SF and dispersion compensation, the system achieves synchronization precision below 200 ps, even in deployed fiber links up to 20 km, by identifying the clock offset $\Delta t = t_{\text{Alice}} - t_{\text{Bob}}$ through cross-correlation peak fitting. While statistical super-localization of the peak position can yield finer estimates under ideal Gaussian conditions, we conservatively report sub-200 ps precision to reflect realistic performance in non-Gaussian, field-deployed scenarios.

E. PERFORMANCE AND SCALABILITY OF FPGA-BASED TCEP SYNCHRONIZATION

The use of FPGAs in our TCEP synchronization system offers several performance benefits, particularly in terms of speed and scalability. By leveraging the FPGA parallel processing architecture, we can perform real-time photon correlation calculations with minimal latency, even when processing large volumes of detection events. The scalability of the system is further enhanced by the FPGA's ability to handle increasing amounts of data without significant degradation in performance, making it well suited for larger, more complex quantum networks.

V. OPENCL

Implementing the cross-correlation function for TCEP leverages the OpenCL framework [27], utilizing its versatility to execute kernels efficiently on an FPGA platform via Intel's software development kit.

OpenCL is a parallel computing application programming interface that facilitates the execution of computational kernels across various platforms, including CPUs, GPUs, and FPGAs. This cross-platform capability allows developers to write a single program that can be deployed on different hardware architectures with minimal changes. By supporting optimization techniques specific to each platform, OpenCL maximizes performance for the underlying hardware. Its parallel computing approach further accelerates computation-intensive applications, making it particularly suited for real-time systems like TCEP-based synchronization.

The OpenCL execution model is based on a heterogeneous computing architecture comprising a host and one or more compute devices (CDs). The host functions as the central controller, responsible for managing memory, task scheduling, and communication with the CDs. These CDs, ranging

IEEE Transactions on Quantum Engineering

from general-purpose CPUs to high-performance accelerators, such as GPUs, DSPs, and FPGAs, execute OpenCL kernels, which are parallelized functions optimized for intensive computational tasks. This architectural flexibility allows developers to leverage the most suitable hardware for a given workload, balancing performance, power efficiency, and scalability. In the context of TCEP-based synchronization, OpenCL provides a robust framework for implementing the cross-correlation function with high precision and low latency, enabling real-time processing critical for accurate clock alignment across distributed quantum nodes.

VI. TESTBED SETUP

A. PHOTON SOURCE AND EMISSION

In this work, entangled photon pairs were generated using the SPDC process. SPDC produces signal and idler photons from a high-energy pump photon interacting with a nonlinear crystal. These photons are temporally correlated, forming the foundation for achieving precise synchronization between spatially separated nodes.

The experiment utilized a continuous-wave (CW) laser operating at 785 nm (Toptica DLC DL PRO 780 FD2 S) to pump a periodically poled potassium titanyl phosphate (ppKTP) nonlinear crystal in a beam-displacer configuration, producing polarization-entangled photons with a broad spectrum around 1550 nm. This wavelength was selected for its high generation rates and superior transmission properties through standard single-mode optical fibers [32]. The SPDC process in the ppKTP crystal produced time-correlated photon pairs at a raw generation rate of approximately 10^6 pairs per second, which could be increased by a factor of up to 10 by adjusting the laser pump power. The spectral properties can be tuned by changing the crystal temperature, which was carefully selected to 33 °C in order to produce spectrally separable photons below and above 1550 nm. This enabled us to use a coarse wavelength division demultiplexer (CWDM) to separate the photons from each other and guide them toward Alice and Bob. As a result, both photons show a spectral width of about 20 nm, which corresponds to the CWDM channel width. The entangled photon source featured an average heralding efficiency of about 20%. The entangled photons were transmitted via single-mode fibers to two remote locations, designated as Alice and Bob.

B. OPTICAL PATH AND FIBER MANAGEMENT

Managing the optical path was critical for minimizing timing errors caused by chromatic dispersion. Chromatic dispersion arises when photons of different wavelengths propagate at different velocities through the optical medium, introducing synchronization inaccuracies. In this experiment, standard telecommunication fibers were used, which feature a low but not to be neglected fiber dispersion of 17 ps / nm·km. Advanced dispersion management techniques, such as SF and dispersion compensation modules (DCM), are often used in longer fiber networks to mitigate these effects. SF effectively reduces the linewidth of transmitted photons, thereby minimizing timing uncertainty, while DCM correct for chromatic dispersion across long-distance fibers [13]. While coincidence window adjustments are sometimes used to refine timing data by discriminating nonsynchronous photons, they are ineffective in reducing the inherent broadening of the correlation peak caused by dispersion. For longer distance quantum networks, employing these advanced techniques could significantly enhance synchronization accuracy by maintaining the sharpness of the temporal correlations [34].

In this context, three main effects of the spectral linewidth on timing accuracy have to be considered.

1) SF will increase the coherence time and therefore also increase the timing uncertainty.
2) The reduced spectral linewidth will also decrease the effects of fiber dispersion, which, otherwise, and for broad spectra, have dramatic effects on the width of the correlation peak and hence reduce timing accuracy. For example, a standard telecom fiber of 20 km in length results in approximately 7-ns broadening of the correlation peak width due to fiber dispersion for photons at 1550 nm and a spectral width of 20 nm.
3) SF also reduces the number of photons contributing to the amplitude of the correlation peak, which reduces the accuracy of super localization of the peak position and therefore also the timing accuracy.

To demonstrate the effect of fiber dispersion, we collected data for five different fiber connection scenarios, which are summarized in Table 1, where a coincidence window of 500 ps was used to estimate the number of correlated pairs. Thereby, the scenario with a short fiber connection of a few meters ensured minimal dispersion effects, preserving the temporal correlations of the entangled photon pairs. This scenario can be seen as the ideal case in terms of synchronization accuracy. For the other scenarios with fiber lengths of 10 and 20 km, respectively, a strong effect of SF and applying a dispersion compensating module on the timing accuracy can be seen.

The 10- and 20-km transmission scenarios use commercial darkfibers deployed in an urban environment, thus demonstrating the practical applicability.

C. PHOTON DETECTION AND FPGA-BASED TIMING ANALYSIS

Photon detection was performed using SNSPDs, IDQuantique, chosen for their high detection efficiency and exceptionally low timing jitter, measured as low as 13 ps (RMS) [17]. In our case, the SNSPDs (ID281) feature a photon detection efficiency $> 85\%$ and an RMS jitter < 50 ps according to the factory and customer acceptance test report. Photon arrival times were recorded at Alice and Bob using picosecond-resolution TDC (quTAG MC, qutools GmbH) with RMS jitter < 20 ps, resulting in an overall single-channel rms jitter < 55 ps. The obtained raw arrival time data

TABLE 1. Fiber Connection and Dispersion Compensation Scenarios

Cases	Length (km)	Fiber Loss Alice/Bob (dB)	SF	DCM	σ (ps)	Coincidences (pairs)	Accidentals	CAR
1	0.002	0/0	no	no	90 ± 1	37556	273	138
2	10	0/10	yes	no	193 ± 2	7258	92	83
3	20	0/16	no	no	1650 ± 30	1118	83	57
4	20	0/20	yes	no	1290 ± 20	1093	43	43
5	20	2/20	yes	yes	174 ± 2	2645	15	176

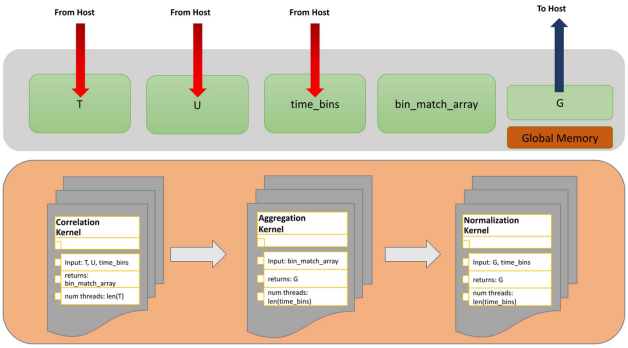

FIGURE 3. OpenCL-based FPGA architecture for real-time TCEP synchronization. Timestamp arrays *T* and *U*, along with user-defined binning information (`time_bins`), are streamed from the host to the FPGA. The *Correlation Processor* assigns detection time pairs to corresponding bins and outputs a `bin_match_array`. This is aggregated by the Accumulation Processor, generating a coarse correlation histogram *G*, which is then refined and normalized by the *Normalization Processor*. The final result *G* is written back to global memory and transferred to the host for peak extraction and synchronization analysis.

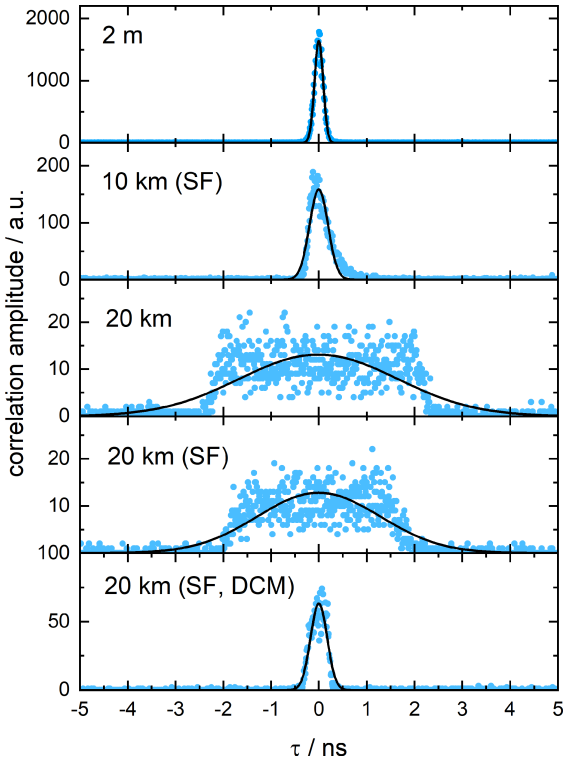

FIGURE 4. Cross correlation for different fiber lengths and compensation methods (SF - SF and DCM - dispersion compensating module) as a function of lagtimes τ for the identification of the time offset between Alice and Bob. The resulting distributions were fitted by a Gaussian function for comparison. The upper data set establishes the baseline system timing jitter in absence of fiber dispersion.

was subsequently processed to determine synchronization offsets between Alice and Bob.

An FPGA-based implementation is utilized to analyze the temporal correlations and calculate the clock offset. The time-stamped photon data are processed using the correlation algorithm specified by [23], and implemented on the FPGA. This algorithm computes the cross-correlation between photon arrival events at Alice and Bob, identifying the peak of the correlation function to determine the synchronization offset.

D. EXPERIMENTAL SETUP AND FPGA INTEGRATION

The experimental setup consisted of two spatially separated nodes, Alice and Bob, connected to a central source of SPDC photons. Entangled photon pairs are transmitted via single-mode fibers to the nodes, which are detected using SNSPDs. The detectors provide time-stamped photon arrival data, which is collected.

The collected time-stamped data is fed into the FPGA, which computes the cross-correlation in real time. A representative plot of the cross correlation is shown in Fig. 4, demonstrating a sharp peak at the clock offset, which was subtracted for comparison with the other datasets. This peak is fitted with a Gaussian function to quantify the synchronization precision. The FPGA implementation achieves a synchronization jitter of below 200 ps for fiber lengths up to 20 km with SF and dispersion compensation, consistent with the timing resolution of the photon detectors and the peak widths reported in Table 1. This performance underscores the system's capabilities for real-time synchronization in high-precision distributed quantum networks.

The FPGA design incorporated three different processing kernels: 1) `correlation`; 2) `aggregation`; and 3) `normalization`. The details of the kernels are described in the following section. The system achieved a clock frequency of approximately 397 MHz, allowing it to efficiently handle large volumes of photon detection events. The details of the kernels are described in the following section.

VII. IMPLMENTATION DETAILS

The DE10-Pro development board equipped with a Stratix 10 FPGA is utilized to implement the quantum postprocessing algorithm. This FPGA platform supports Intel OpenCL

IEEE Transactions on Quantum Engineering

TABLE 2. Description of the Arrays Used in OpenCL FPGA Implementation

Array Name	Description	Size
`T`	Monotonically increasing timestamps (Alice)	`len(T)`
`U`	Monotonically increasing timestamps (Bob)	`len(U)`
`time_bins`	Bin edges for correlation computation	`len(time_bins)`
`bin_match_array`	Partial correlation results	`len(T) * (len(time_bins) - 1)`
`G`	Final correlation results	`len(time_bins) - 1`

board support package, enabling efficient real-time processing of photon timestamp data for TCEP source-based synchronization systems. To accelerate the cross-correlation computation, we implement three OpenCL kernels on the FPGA. Fig. 3 illustrates the top-level design, depicting arrays, and kernel interactions.

1) *Correlation Kernel:* This kernel computes the cross-correlation between timestamps in array `T` and array `U` for all time bins (`time_bins`). Each thread processes one array element of `T` and determines how many elements of `U` fall into specific bins.
2) *Aggregation Kernel:* This kernel accumulates the results from the correlation kernel by summing the partial counts across all timestamps in `T`. The final output, stored in `G`, represents the number of coincidences for each time bin.
3) *Normalization Kernel:* This kernel normalizes the aggregated counts in `G` by dividing each count by the corresponding bin width, ensuring a correct estimation of the cross-correlation function.

Table 2 describes the arrays used in the OpenCL implementation.

The mathematical formulation of correlation computation follows a structured three-step approach as follows.

1) Correlation Computation: For each timestamp $t_i \in \mathtt{T}$, the correlation kernel finds all timestamps $u_j \in \mathtt{U}$ that fall within specific bins:

$$\mathtt{bin\_match\_array}[i][k] = \sum_j \mathbb{1}\{u_j \in [t_i + \tau_k, t_i + \tau_k + \Delta t_k]\} \tag{10}$$

where $\mathbb{1}$ is the indicator function.

2) Aggregation of Matches: The aggregation kernel sums across all timestamps t_i for each bin index k

$$G[k] = \sum_{i=0}^{\mathtt{len(T)}} \mathtt{bin\_match\_array}[i][k]. \tag{11}$$

3) Normalization: To ensure accuracy, the final cross-correlation function is normalized

$$\hat{C}_{AB}(\tau_k) = \frac{G[k]}{\Delta t_k}. \tag{12}$$

This normalization accounts for bin widths, ensuring that correlation values are comparable across different bin sizes.

The OpenCL FPGA implementation is optimized as follows.

1) *Thread-Level Parallelism:* Each timestamp t_i is processed independently to maximize concurrency.
2) *Disaggregating Kernels:* Dividing the operation in different kernels allowed to add parallelism and increasing the operation frequency.
3) *Caching:* Temporary arrays, such as `bin_match_array` are stored in FPGA block RAM (BRAM) to allow fast read/write operations.

VIII. RESULTS AND DISCUSSION

A. CORRELATION ANALYSIS AND EXPERIMENTAL VALIDATION

The FPGA system computes photon correlation in real time, allowing for the continuous evaluation of synchronization offsets in both laboratory (2 m) and long-distance (10 and 20 km) fiber conditions, with or without additional experimental measures, such as SF or a DCM. Fig. 4 and Table 1 show the results for the determination of the time offset between Alice and Bob. The key observations are as follows.

1) In the short in-lab fiber setup ("2 m" fiber length), the coincidence peak is sharply localized and well-approximated by a Gaussian fit with a full-width jitter of 90 ps. This reflects near-ideal correlation conditions with negligible chromatic dispersion.
2) For long-distance fiber links, standard telecommunication fibers introduce significant chromatic dispersion, substantially broadening the correlation peak. In the "20 km" case (see Fig. 4), the temporal spread increases to 1.65 ns.
3) SF, applied as a partial mitigation technique, effectively reduces the impact of dispersion. In the "10 km (SF)" and "20 km (SF)" subplots, the jitter is reduced to approximately 190 ps and 1.3 ns, respectively. Nevertheless, the 20-km configuration remains inadequate for high-precision synchronization applications.
4) Introducing a DCM in addition to SF further sharpens the coincidence peak. In the "20 km (SF, DCM)" scenario, the jitter is reduced to approximately 175 ps—comparable to the near-ideal performance observed in the 2 m in-lab setup. This confirms the efficacy of dispersion compensation in restoring timing resolution over long distances.
5) All scenarios exhibit distinct synchronization peaks with strong amplitude-to-background contrast, demonstrating that the FPGA-based system reliably preserves the temporal correlation structure even under adverse channel conditions.

TABLE 3. Resource Utilization Summary for FPGA Modules

Module	ALMs	Registers	MLABs	RAM Blocks	DSPs
Accumulation Kernel	3261.6	6239	46	37	2
Normalization Kernel	4010.2	8846	59	24	10
Cross-Correlation Kernel	7796.8	15 738	83	116	2
Full Design	31 557.2	67 688	193	389	14
Frequency (MHz)	397.5				

6) The synchronization jitter values of 100–200 ps reported here correspond to averaging periods of 10 Hz or greater. These values assume adequate photon detection rates and sufficiently low fiber attenuation to enable accurate extraction of the cross-correlation peak.
7) These results confirm the feasibility of TCEP-based synchronization and demonstrate the effectiveness of the FPGA implementation in compensating for timing dispersion over optical fiber links, an essential requirement for the practical deployment of real-world quantum networks.

The method can compensate for local clock drifts (for example, on the order of roughly 1 μs/s for a temperature-controlled crystal oscillator), providing the indicated synchronization accuracy. For a successful synchronization, it is sufficient that within a time window well below the nonlinear relative clock drift, a sufficient number of true coincidences is measured between the communicating parties. Also, in the case of drifting optical path lengths (for example, due to temperature effects), the present method can provide a frequency synchronization from the time distance between two consecutive photon pairs. This is possible because the time scale of the drifts is many magnitudes larger than the photon transmission times and the offset determination bin widths.

B. KERNEL PERFORMANCE AND RESOURCE UTILIZATION

The system design effectively utilized the FPGA modular architecture to process timestamped photon data efficiently. Resource utilization across the primary modules is summarized in Table 3.

The cross-correlation kernel was the most resource-intensive, consuming 7796.8 ALMs and 15 738 registers to support real-time temporal correlation computations. In comparison, the normalization and accumulation kernels required fewer resources, i.e., 4,010.2 ALMs and 8846 registers, and 3261.6 ALMs and 6239 registers, respectively, reflecting their more lightweight processing roles. The complete design, which integrates all modules, utilizes 31 557.2 ALMs, 67 688 registers, and 389 RAM blocks, highlighting the scalability and feasibility of the architecture for larger quantum network deployments.

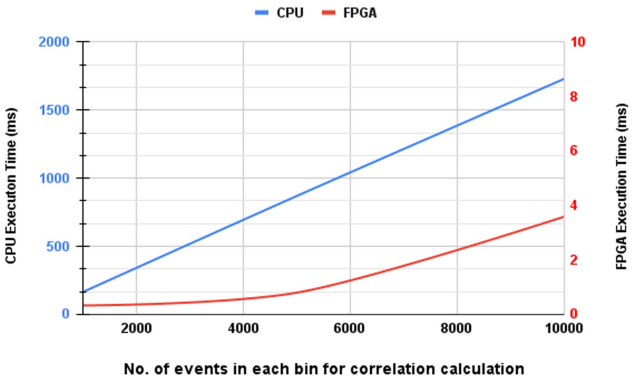

FIGURE 5. Comparison of execution times for FPGA- and CPU-based implementations across varying bin sizes for a short fiber length of approximately 2 m. The FPGA consistently achieves real-time performance, even at high event counts (100 000 timestamps).

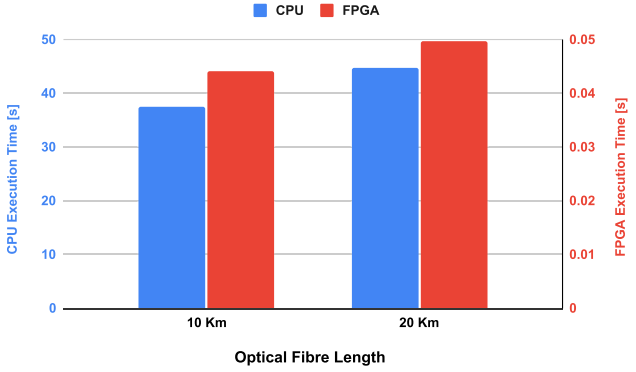

FIGURE 6. Execution time comparison of CPU vs. FPGA implementation for different fiber lengths (fixed bin size = 2000). The FPGA maintains consistent execution latency (~50 ms), while CPU time increases to over 40 s for 20 km.

C. EXECUTION TIME ANALYSIS

To evaluate the performance of the proposed system, execution times are measured and compared between an FPGA-based implementation and a traditional CPU-based approach across various time bin sizes.

Fig. 5 highlights, across all tested bin sizes, the FPGA consistently outperforms the CPU in correlation tasks—often by more than an order of magnitude—due to its parallel architecture and dedicated hardware resources. Even at large scales (e.g., 10 000 events), the FPGA maintains sub-10-ms processing times, while the CPU exceeds 1500 ms. This demonstrates the FPGA's suitability for real-time, high-throughput synchronization applications.

To further evaluate execution latency in realistic link scenarios, we measured correlation performance as a function of optical fiber length. For both 10 and 20 km fibers (with a fixed bin size of 2000), the FPGA maintained latency of 44.0 and 50.0 ms, respectively. In contrast, the CPU required 37.4 and 44.7 s for the same configurations.

Two key factors influence the overall synchronization latency between two nodes. First, timestamp data must

be transferred between the nodes or to an intermediate processing station, which can be efficiently handled via high-speed classical networks. Second, the delay arises from the computation of cross correlation itself. While this takes approximately 44.7 s on a conventional CPU for a 20 km (SF+DCM) setup, the same computation is accelerated to just 50.0 ms using our FPGA-based implementation.

This represents a consistent $\sim 800\times$ acceleration using FPGA over CPU, with minimal performance degradation over increased channel length, highlighting the significant performance advantage of hardware acceleration for real-time synchronization. These results highlight the scalability and robustness of our hardware platform for synchronization in distributed quantum networks.

IX. CONCLUSION

This study establishes TCEP-based synchronization as a scalable and precise solution for achieving subnanosecond timing accuracy in distributed quantum networks. By leveraging the strong temporal correlations of entangled photon pairs, the system achieved synchronization jitter below 100 ps for short fiber connections and below 200 ps for a 20-km fiber link with SF and dispersion compensation. Experimental validation demonstrated real-time processing of large-scale photon timestamp datasets on FPGA, achieving millisecond-range execution times even for high-resolution temporal bins. These findings highlight the suitability of TCEP-based synchronization for applications requiring URLLC and secure quantum protocols, such as QKD. Compared to classical methods, the quantum nature of TCEP offers inherent resilience to environmental perturbations, robust operation under fiber-induced drift, and scalability for large quantum networks.

Subnanosecond-precision synchronization for distant clocks via TCEP presents significant advancements for future quantum and classical networks, autonomous systems, navigation, financial applications, and the exploration of fundamental science. By distributing the timing reference using correlated photons, TCEP enables resilient, decentralized synchronization suitable for dynamic and heterogeneous network environments. Ongoing enhancements in FPGA power efficiency will promote widespread adoption, establishing TCEP as a critical technology for bridging quantum capabilities with real-world time sensitive applications.

REFERENCES

[1] D. W. Allan, "Time and frequency(time-domain) characterization, estimation, and prediction of precision clocks and oscillators," *IEEE Trans. Ultrasonics, Ferroelectrics, Freq. Control*, vol. 34, no. 6, pp. 647–654, Nov. 1987, doi: 10.1109/T-UFFC.1987.26997.

[2] B. Baghdasaryan and S. Fritzsche, "Enhanced entanglement from Ince-Gaussian pump beams in spontaneous parametric down-conversion," *Phys. Rev. A*, vol. 102, no. 5, 2020, Art. no. 052412, doi: 10.1103/PhysRevA.102.052412.

[3] B. Baghdasaryan, C. Sevilla-Gutiérrez, F. Steinlechner, and S. Fritzsche, "Generalized description of the spatio-temporal biphoton state in spontaneous parametric down-conversion," *Phys. Rev. A*, vol. 106, no. 6, 2022, Art. no. 063711, doi: 10.1103/PhysRevA.106.063711.

[4] K. Balakrishnan, R. Dhanalakshmi, and R. Gopalakrishnan, "Clock synchronization in industrial Internet of Things and potential works in precision time protocol: Review, challenges and future directions," *Int. J. Cogn. Comput. Eng.*, vol. 4, pp. 205–219, 2023, doi: 10.1016/j.ijcce.2023.06.001.

[5] S. Brown and J. Rose, "FPGA and CPLD architectures: A tutorial," *IEEE Des. Test Comput.*, vol. 13, no. 2, pp. 42–57, Summer 1996, doi: 10.1109/54.500200.

[6] *Precision Clock Synchronization Protocol for Networked Measurement and Control Systems*, IEEE Standard 1588, 2004, doi: 10.1109/IEEESTD.2008.4579760.

[7] J. C. Corbett et al., "Spanner: Google's globally distributed database," *ACM Trans. Comput. Syst.*, vol. 31, no. 3, pp. 1–22, 2013, doi: 10.1145/2491245.

[8] P. H. Dana and B. M. Penrod, "The role of GPS in precise time and frequency dissemination," *GPS World*, vol. 1, no. 4, pp. 38–43, 1990. [Online]. Available: https://ilrs.gsfc.nasa.gov/docs/timing/gpsrole.pdf

[9] D. L. Mills, *Computer Network Time Synchronization: The Network Time Protocol on Earth and in Space*. CRC Press Raton, FL, USA, 2017, doi: 10.1201/b10282.

[10] J. C. Eidson, M. Fischer, and J. White, "IEEE-1588 standard for a precision clock synchronization protocol for networked measurement and control systems," in *Proc. 34th Annu. Precise Time Time Interval Syst. Appl. Meeting*, 2002, pp. 243–254. [Online]. Available: https://www.ion.org/publications/abstract.cfm?articleID=13942

[11] A. Einstein, B. Podolsky, and N. Rosen, "Can quantum-mechanical description of physical reality be considered complete?," *Phys. Rev.*, vol. 47, no. 10, 1935, Art. no. 777, doi: 10.1103/PhysRev.47.777.

[12] C. Farabet et al., "Large-scale FPGA-based convolutional networks," *Scaling Mach. Learn.: Parallel Distrib. Approaches*. Cambridge, U.K.: Cambridge Univ. Press, vol. 13, no. 3, pp. 399–419, 2011.

[13] S. Fasel, N. Gisin, G. Ribordy, and H. Zbinden, "Quantum key distribution over 30 km of standard fiber using energy-time entangled photon pairs: A comparison of two chromatic dispersion reduction methods," *Eur. Phys. J. D-Atomic, Molecular, Opt. Plasma Phys.*, vol. 30, pp. 143–148, 2004, doi: 10.1140/epjd/e2004-00080-8.

[14] V. Giovannetti, S. Lloyd, and L. Maccone, "Quantum-enhanced positioning and clock synchronization," *Nature*, vol. 412, no. 6845, pp. 417–419, 2001, doi: 10.1038/35086525.

[15] V. Giovannetti, S. Lloyd, and L. Maccone, "Advances in quantum metrology," *Nature Photon.*, vol. 5, no. 4, pp. 222–229, 2011, doi: 10.1038/nphoton.2011.35.

[16] J. L. Gutiérrez-Rivas, F. Torres-González, E. Ros, and J. Díaz, "Enhancing white rabbit synchronization stability and scalability using P2P transparent and hybrid clocks," *IEEE Trans. Ind. Inform.*, vol. 17, no. 11, pp. 7316–7324, Nov. 2021, doi: 10.1109/TII.2021.3054365.

[17] R. H. Hadfield, "Single-photon detectors for optical quantum information applications," *Nature Photon.*, vol. 3, no. 12, pp. 696–705, 2009, doi: 10.1038/nphoton.2009.230.

[18] C. K. Hong and L. Mande, "Theory of parametric frequency down conversion of light," *Phys. Rev. A*, vol. 31,, no. 4, 1985, Art. no. 2409, doi: 10.1103/PhysRevA.31.2409.

[19] J. Huang, M. Zhuang, and C. Lee, "Entanglement-enhanced quantum metrology: From standard quantum limit to Heisenberg limit," *Appl. Phys. Rev.*, vol. 11, no. 3, 2024, Art. no. 031302, doi: 10.1063/5.0204102.

[20] R. Jozsa, D. S. Abrams, J. P. Dowling, and C. P. Williams, "Quantum clock synchronization based on shared prior entanglement," *Phys. Rev. Lett.*, vol. 85,, no. 9, 2000, Art. no. 2010, doi: 10.1103/PhysRevLett.85.2010.

[21] K. Kapoor et al., "Picosecond synchronization of photon pairs through a fiber link between Fermilab and Argonne national laboratories," *IEEE J. Quantum Electron.*, vol. 59, no. 4, Aug. 2023, Art. no. 9300107, doi: 10.1109/JQE.2023.3240756.

[22] I. Kuon and J. Rose, "Measuring the gap between FPGAS and ASICS," in *Proc. ACM/SIGDA 14th Int. Symp. Field Programmable Gate Arrays*, 2006, pp. 21–30, doi: 10.1145/1117201.1117205.

[23] T. A. Laurence, S. Fore, and T. Huser, "Fast, flexible algorithm for calculating photon correlations," *Opt. Lett.*, vol. 31, no. 6, pp. 829–831, 2006, doi: 10.1364/OL.31.000829.

[24] A. Lyons et al., "Attosecond-resolution Hong-Ou-Mandel interferometry," *Sci. Adv.*, vol. 4, no. 5, 2018, Art. no. eaap9416, doi: 10.1126/sciadv.aap9416.

[25] D. L. Mills, "Internet time synchronization: The network time protocol," *IEEE Trans. Commun.*, vol. 39, no. 10, pp. 1482–1493, Oct. 1991, doi: 10.1109/26.103043.

[26] P. Moreira, J. Serrano, T. Wlostowski, P. Loschmidt, and G. Gaderer, "White rabbit: Sub-nanosecond timing distribution over ethernet," in *Proc. Int. Symp. Precis. Clock Synchronization Meas., Control Commun.*, 2009, pp. 1–5, doi: 10.1109/ISPCS.2009.5340196.

[27] A. Munshi, B. Gaster, T. G. Mattson, and D. Ginsburg, *OpenCL Programming Guide*. Pearson Education London, U.K.:, 2011, doi: 10.5555/2049883.

[28] S. S. Nande, A. Garbugli, R. Bassoli, and F. H. P Fitzek, "Time synchronization in communication networks: A comparative study of quantum technologies," in *Proc. IEEE Wireless Commun. Netw. Conf.*, 2024, pp. 1–6, doi: 10.1109/WCNC57260.2024.10570688.

[29] V. Scarani, H. Bechmann-Pasquinucci, N. J. Cerf, M. Dušek, N. Lütkenhaus, and M. Peev, "The security of practical quantum key distribution," *Rev. Modern Phys.*, vol. 81, no. 3, pp. 1301–1350, 2009, doi: 10.1103/RevModPhys.81.1301.

[30] J. Serrano et al., "The white rabbit project," in *Proc. 2nd Int. Beam Instrum. Conf.*, 2013.

[31] C. Spiess et al., "Clock synchronization with correlated photons," *Phys. Rev. Appl.*, vol. 19, no. 5, 2023, Art. no. 054082, doi: 10.1103/PhysRevApplied.19.054082.

[32] S. W. Tanzilli eta al., "PPLN waveguide for quantum communication," *Eur. Phys. J. D-Atomic, Molecular, Opt. Plasma Phys.*, vol. 18, pp. 155–160, 2002, doi: 10.1140/epjd/e20020019.

[33] F. Torres-González, J. Díaz, E. Marín-López, and R. Rodriguez-Gómez, "Scalability analysis of the white-rabbit technology for cascade-chain networks," in *Proc. IEEE Int. Symp. Precis. Clock Synchronization Measurement, Control, Commun.*, 2016, pp. 1–6, doi: 10.1109/ISPCS.2016.7579515.

[34] A. Valencia, G. Scarcelli, and Y. Shih, "Distant clock synchronization using entangled photon pairs," *Appl. Phys. Lett.*, vol. 85, no. 13, pp. 2655–2657, 2004, doi: 10.1063/1.1797561.

[35] J. R. Vig, "Quartz crystal resonators and oscillators for frequency control and timing applications. A tutorial," *NASA STI/recon Tech. Rep. N*, vol. 95, 1994, Art. no. 19519, doi: 10.13140/2.1.2134.0962.

[36] S. Wengerowsky, S. K. Joshi, F. Steinlechner, H. Hübel, and R. Ursin, "An entanglement-based wavelength-multiplexed quantum communication network," *Nature*, vol. 564, pp. 225–228, 2018, doi: 10.1038/s41586-018-0766-y.

[37] J. Xu, K. Li, and Y. Chen, "Real-time task scheduling for FPGA-based multicore systems with communication delay," *Microprocessors Microsystems*, vol. 90, 2022, Art. no. 104468, doi: 10.1016/j.micpro.2022.104468.

[38] R. Zarick, M. Hagen, and R. Bartoš, "The impact of network latency on the synchronization of real-world ieee 1588-2008 devices," in *Proc. IEEE Int. Symp. Precis. Clock Synchronization Meas., Control Commun.*, 2010, pp. 135–140, doi: 10.1109/ISPCS.2010.5609788.

[39] Y.-L. Zhang, Y.-R. Zhang, L.-Z. Mu, and H. Fan, "Criterion for remote clock synchronization with Heisenberg-scaling accuracy," *Phys. Rev. A–Atomic, Mol., Opt. Phys.*, vol. 88, no. 5, 2013, Art. no. 052314, doi: 10.1103/PhysRevA.88.052314.